Dyes and Pigments 196 (2021) 109553

Contents lists available at ScienceDirect

Dyes and Pigments

journal homepage: www.elsevier.com/locate/dyepig

CytoCy5S™, a compound of many structures. *in vitro* and *in vivo* evaluation of four near-infrared fluorescent substrates of nitroreductase (NTR)

Elvira García de Jalón [a,b], Gorka Ruiz de Garibay [a,c,d], Bengt Erik Haug [b,**], Emmet McCormack [a,e,f,*]

[a] Centre for Cancer Biomarkers CCBIO, Department of Clinical Science, The University of Bergen, Jonas Lies Vei 65, Bergen, 5021, Norway
[b] Department of Chemistry and Centre for Pharmacy, University of Bergen, Allégaten 41, N-5007, Bergen, Norway
[c] University Hospital 12 de Octubre, Madrid, Spain
[d] Lung Cancer Unit H12O-CNIO, Madrid, Spain
[e] Centre for Pharmacy, Department of Clinical Science, The University of Bergen, Jonas Lies Vei 65, Bergen, 5021, Norway
[f] Vivarium, Department of Clinical Medicine, The University of Bergen, Jonas Lies Vei 65, 5021, Bergen, Norway

ARTICLE INFO

Keywords:
CytoCy5S
Cyanine
Squaraine
Nitroreductase
NfsB
Near-infrared fluorescence imaging

ABSTRACT

CytoCy5S™, a quenched, red-shifted fluorescent probe, has been used to exploit the imaging potential of the nitroreductase (NTR) reporter gene platform. Its use has been reported in a number of publications, however there are discrepancies in both the reported structure and its physicochemical properties. Herein, we aim to highlight these discrepancies and to define the best candidate of the four substrates under study for preclinical work in NTR reporting by optical applications.

We report the synthesis, purification and characterisation of four NTR substrates, including alternately described structures currently referred by the name CytoCy5S. A comparative NTR enzymatic assay was performed to assess the spectroscopic characteristics of the different reductively activated probes. The NTR expressing triple-negative breast carcinoma cell line, MDA-MB-231 NTR^{+}, was employed to compare, both *in vitro* and *in vivo*, the suitability of these fluorescent probes as reporters of NTR activity. Comparison of the reporting properties was achieved by flow cytometry, fluorescence microscopy and optical imaging, both *in vivo* and *ex vivo*.

This study evaluated the different spectroscopic and biological characteristics of the four substrates and concluded that substrate **1** presents the best features for oncological *in vivo* preclinical optical imaging.

1. Introduction

Fluorescence imaging (FLI) is a non-invasive, easy to perform and cheap imaging modality permitting real-time visualisation, which has become fundamentally important in preclinical studies of oncological malignancies [1]. This technique relies on the detection of the light emitted directly by an exogenous fluorescent probe, endogenous reporter gene or indirectly by the combination of a reporter gene and its corresponding fluorescent substrate. By employing an appropriate selection of reporter genes, FLI can be used to assess anatomical location of tumour cells and ongoing biological processes [2,3].

Of particular relevance in biological applications is the exploitation of the near-infrared (NIR) region of the electromagnetic spectrum (650–950 nm) [4,5]. This privileged region is characterised by reduced tissue absorption caused by haemoglobin or melanin and deeper tissue penetration compared to the visible region [6,7]. Non-invasive FLI using NIR dyes has proven to be a very useful tool in preclinical oncology models for detection of metastasis and treatment response monitoring in orthotopic models [8] and has been widely explored in both preclinical and clinical settings for fluorescence image-guided surgery [9–12]. A number of fluorescent probes that emit light in the NIR region such as phthalocyanines [13], porphyrins [14] or BODIPY dyes [15] (Fig. 1A I–III) have been employed as contrast agents or theranostics. However, so far cyanines and their squaraine analogues (Fig. 1A IV–V) have been the preferred NIR dyes for the study of oncological conditions [4,16].

One limitation of these “always-on” probes is the accumulation of

* Corresponding author. Centre for Cancer Biomarkers CCBIO, Department of Clinical Science, The University of Bergen, Jonas Lies vei 65, Bergen, 5021, Norway.
** Corresponding author. Department of Chemistry and Centre for Pharmacy, University of Bergen, Allégaten 41, N-5007, Bergen, Norway.
E-mail addresses: Bengt-Erik.Haug@uib.no (B.E. Haug), emmet.mc.cormack@uib.no (E. McCormack).

https://doi.org/10.1016/j.dyepig.2021.109553
Received 12 January 2021; Received in revised form 6 May 2021; Accepted 5 June 2021
Available online 15 June 2021

background fluorescence in off-target tissues that limits the detection of the pathology under study. To overcome this challenge, activatable probes that are specifically activated at the pathology of interest are employed, providing better contrast that allows non-invasive FLI of different biological processes associated with tumour growth [18–21].

Several examples can be found where reductive properties of nitroreductases (NTR) have been exploited for non-invasive FLI of tumorigenesis and hypoxia in tumour cells [22,23] but also of bacterial infections and response to antibiotics [24–26], among others [27]. Furthermore, the NTR reporter gene can be exploited as a suicide gene, in a gene directed enzyme prodrug therapy setting (GDEPT), with high potential as a theranostic agent, affording therapy and therapy efficacy visualisation simultaneously [8,28]. NTR-activatable probes, including CytoCy5S [29] or 6-chloro-9-nitro-5-oxo-5*H*-benzo[a]phenoxazine (CNOB) [30], are non-fluorescent prior to enzymatic metabolism and become highly fluorescent after the catalytic reaction. These NTR-activatable probes contain aromatic nitro groups that render them non-fluorescent. However, reduction of the nitro groups to the corresponding hydroxylamines and/or amines by nitroreductases in the presence of FMN and NADH and NADPH restores fluorescence (Fig. 2) [31,32].

CytoCy5S is the most extensively utilised NTR-activatable fluorescent probe. This compound has been widely exploited for different purposes [8,24,33–36] and despite its promising performance, there is a discrepancy in the literature with respect to its structure, as both **1** and **4** (Fig. 1B) have been referred to as CytoCy5S [37–39]. Both structures contain a 3,5-dinitrobenzyl moiety, but while **1** is a squaraine derivative, **4** is a cyanine derivative. Consequently, there is also a lack of consensus in the literature regarding the spectroscopic properties and its behaviour in biological systems, which might hamper its use. The manufacturer describes CytoCy5S as a hydrophobic molecule, with limited availability in aqueous buffers, and with improved cell permeability [40], however Parker et al. [41] describe CytoCy5S as a photo-stable and water soluble compound. Furthermore, the reduced version of CytoCy5S is described by the manufacturer as a red-shifted substrate with excitation at 628 nm and emission at 638 nm [40], while Inglese et al. [42] reports the excitation and emission maxima for the reduced version to be 647 nm and 667 nm, respectively. No information on the structure was included [40,42]. In our previous work, the final reduction product of **1** revealed excitation and emission maxima of 631 and 688 nm, respectively [8]. Finally, in a recent review [43], compound **4** is proposed as CytoCy5S and the version we employed in the aforementioned work [8], **1**, is described as a squaraine analogue of **4**.

Based on these discrepancies in the literature [8,24,33,37,40,41,43],

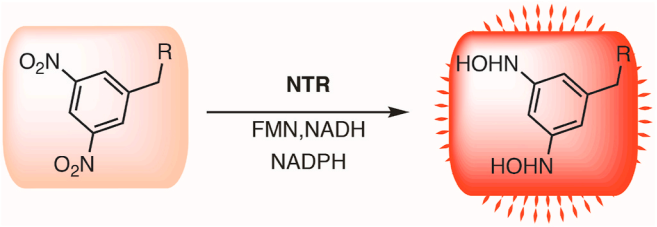

Fig. 2. NTR-mediated reduction of aromatic nitro groups
NTR-mediated reduction of substrates **1**–**4** in the presence of FMN (bound to NTR) and NADH and NADPH to give the proposed product and restore fluorescence.

we decided to compare four different NTR-activatable probes, two of them the alternative versions of CytoCy5S found in the literature. In addition, we included compound **2** (squaraine) as we believe that this compound might also have been used as CytoCy5S, however, also in order to investigate how the carboxylic acid tail that is present in both compounds **1** and **4** affects its behaviour in a biological system. Finally, we included compound **3** (squaraine) [37] since this NTR substrate was found to have superior spectroscopic properties to that of compound **1** in an *in vitro* screening of different contrast agents (unpublished data). The four probes (Fig. 1B) were synthesised and analysed *in vitro* and *in vivo* in order to shed light on their performance and properties with the intention of identifying the most suitable NIR dye for biological imaging of NTR.

2. Materials and methods

2.1. Synthesis and characterisation of dyes *1 - 4*

Detailed protocols for the synthesis of **1**–**4** and investigations into increasing the yield for the synthesis of **1** are provided in the electronic supplementary material.

2.2. NTR enzymatic assays

A mixture containing 4.5% DMSO, 60 μM β-NADH in 10 mM Tris-HCl and 0.98 mM β-NADPH in 10 mM Tris-HCl was prepared and the reaction mixture completed as follows: For the blank, Tris-HCl 10 mM quantum satis (q.s.) and 0.2 μM NTR were added. For the references, 4 μM of either of **1**–**4** (in 90% DMSO and 10% Tris-HCl 100 mM) q.s. was added. And for the study sample, 4 μM of either of **1**–**4** (in 90% DMSO and 10% Tris-HCl 100 mM) q.s. and 0.2 μM NTR were added (all

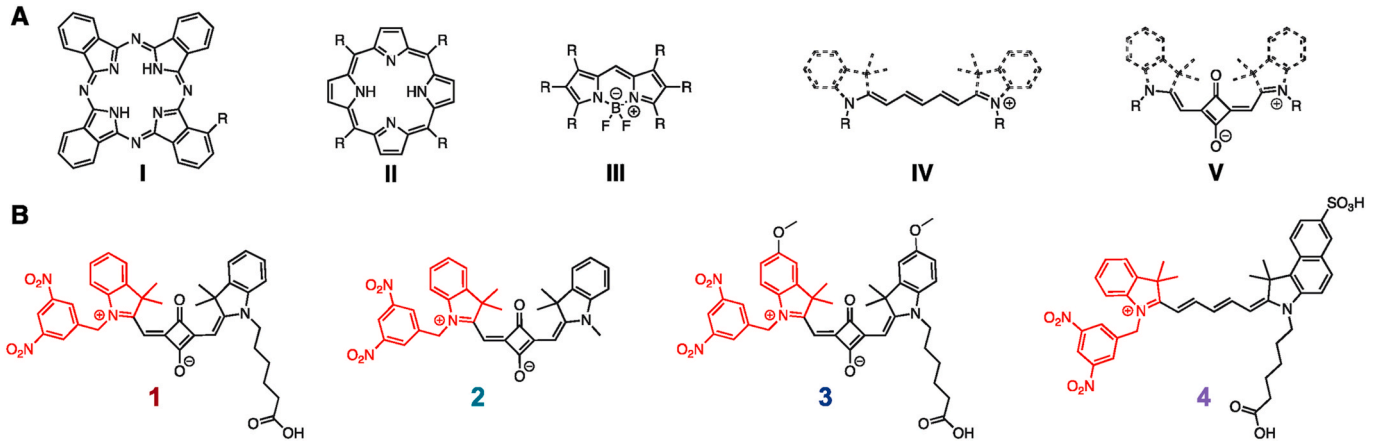

Fig. 1. Common scaffolds employed for molecular interrogation in biological applications.
A) Phthalocyanine (**I**), porphyrin (**II**), BODIPY (**III**), cyanine structure (**IV**), squaraine structure (**V**). **B)** Different substrates evaluated in this study. Structures **1** and **4** referred as CytoCy5S in the literature. (Structures are represented in their *cis* conformation although this is not the most stable one [17]).

reagents added in the stated order). After a 2-h reaction, the excitation and emission spectra of the different dyes reductively activated by NTR were acquired. Excitation and absorbance scans were performed from 500 to 700 nm and emission scans from 600 to 800 nm in 2 nm steps and a 20 nm bandwidth in both cases.

The optimal settings for excitation and emission were then used to measure the fluorescence intensity during the course of the enzymatic reactions (up to 24 h). The optimal settings for the different substrates were defined as follows: substrates **1** and **2**: $\lambda_{ex}/\lambda_{em}$ 630/645 nm; substrate **3**: $\lambda_{ex}/\lambda_{em}$ 650/670 nm; substrate **4**: $\lambda_{ex}/\lambda_{em}$ 660/690 nm; 5 nm bandwidth in all cases. Fluorescence intensity was analysed using a Tecan Spark® multimode microplate reader (Tecan Group Ltd., Männedorf, Switzerland) and data was plotted as the average ± SD.

2.3. Cell lines and cell culture

The human mammary carcinoma cell line MDA-MB-231 was employed for *in vitro* and *in vivo* assays. MDA-MB-231^{Luc+} (NTR^-) cells were kindly provided by Prof. James Lorens (University of Bergen) and MDA-MB-231$^{Luc\ +\ GFP\ +\ NTR+}$ (NTR^+) cells have been generated in our lab as previously reported by McCormack et al. [8]. All cell types were cultured in DMEM (Sigma-Aldrich, Merck KGaA, Darmstadt, Germany) supplemented with 10% FBS and 1% L-glutamine (Sigma-Aldrich) in a humidified atmosphere at 37 °C and 5% CO_2.

2.4. Flow cytometry

Comparative quantification of the fluorescence intensities obtained with the different substrates was performed by incubating 1×10^5 of the NTR^+ and NTR^- cells (negative control) with each of them. First, different substrate concentrations (1 μM, 3 μM, 12 μM, 25 μM) were tested, by incubating the cells for 1 h. Once the best concentration was identified, different incubation times were assessed in triplicate (0.25 h, 0.5 h, 1 h, 2 h, 4 h and 8 h). In all cases, after the incubation time the cells were rinsed with PBS, trypsinised and washed twice before resuspension in PBS supplemented with 2% BSA. Acquisition was performed in a BD LSR Fortessa flow cytometer (BD Biosciences, Franklin Lakes, NJ, USA) with a 640 nm excitation laser and a 670 ± 14 nm emission filter. The voltage of the detector was optimised for the brightest signal and kept at the optimal setting for all the different experiments.

2.5. Fluorescence microscopy

1×10^5 NTR^+ cells were seeded in 35 mm μ-dishes with high glass bottom (Ibidi, Martinsried, Germany) and were incubated with 3 μM of each individual substrate for 10 min. Uptake, fluorescence release and the fate of the reduced substrates in the cell was followed at 10 min intervals for up to 4 h. Cells were maintained at 37 °C and 5% CO_2. Live cell imaging fluorescence was acquired using a confocal Andor Dragonfly microscope (Oxford Instruments America, Inc., Concord MA, USA) with a 40X magnification, with the 488 nm excitation filter and green emission filter (500–550 nm) for GFP expression and the 637 nm excitation filter and the far red emission filter (663–738 nm) for NTR interrogation. All data collected were analysed with Imaris 9.6 (Oxford Instruments, USA).

2.6. General animal care

All applicable institutional and/or national guidelines for the care and use of animals were followed. All experiments were approved by The Norwegian Animal Research Authority (Application ID 14128) and conducted according to The European Convention for the Protection of Vertebrates Used for Scientific Purposes. NOD-*scid* IL2Rg^{null} mice (referred to as NSG) were bred at Vivarium (University of Bergen) from breeding pairs purchased from Charles River. Mice were housed in groups of ≤5 in individually ventilated cages (Techniplast S.p.A., Buguggiate, Italy). Observations for general condition and body weights were recorded twice a week. Mice were fed with low-autofluorescence rodent imaging food (Rodent imaging diet D1001 from Research diets Inc., Brunswick, USA) from, at least, two weeks prior to experiments. Mice were depilated prior to image acquisition. When required, mice were anesthetised under 1.5% isoflurane (Abbot Laboratories Ltd., North Chicago, USA). Mice were euthanised according to institutional guidelines.

2.7. MDA-MB-231 subcutaneous xenografts

NTR^- and NTR^+ MDA-MB-231 subcutaneous xenografts were implanted in the left flank of the scapular area by injection of 5×10^6 cells suspended in 100 μL DMEM with 25% Matrigel (Corning Inc., Waltham, USA). Tumour volumes were measured weekly with a digital calliper and calculated using the ellipsoid volume formula: Volume = π (length x width x height)/6.

2.8. in vivo fluorescence imaging

2.8.1. in vivo biodistribution

For biodistribution and pharmacokinetic assessment of the four different substrates, when mean tumour volumes reached 120 ± 16 mm^3, mice were intravenously injected with 100 μL of a 1 mM substrate solution. Optical imaging was performed at established time points (0 h, 0.75 h, 2 h, 4 h, 8 h, 12 h and 24 h) using an IVIS Spectrum imaging system (PerkinElmer Inc., Waltham, USA) with the following filter pairs ($\lambda_{ex}/\lambda_{em}$) 640/680 and 640/700 nm. To assess the background fluorescence, all mice were imaged prior to injection. Analysis of the collected data was performed with the Living Imaging® software v4.5 (PerkinElmer Inc.). Regions of interest (ROI) in the lateral view were manually drawn around the tumours and fluorescence was expressed as radiance (p/s/cm^2/sr). The radiance values reported were normalised by the mean of the NTR^- radiance values.

2.8.2. Longitudinal tumour imaging

Tumours were longitudinally imaged three times over the course of the tumour progression. Imaging acquisitions were performed when the mean tumour volumes reached 222 ± 44 mm^3, 300 ± 71 mm^3 and 451 ± 115 mm^3. 100 μL of a 1 mM substrate solution were injected intravenously and images were acquired after 0.75 h for **1** and **3** and after 2 h for **2** using an IVIS Spectrum imaging system with λ_{ex} = 640 nm and λ_{em} = 680 nm. To assess the background fluorescence, all mice were imaged prior to injection. Analysis of the collected data was performed as explained before. The radiance values reported were normalised by the mean of the NTR^- radiance values.

2.8.3. ex vivo biodistribution

Mice were euthanised 0.75 h after i.v. administration of **1** and **3** and 2 h after i.v injection of **2** (100 μL, 1 mM) and tumours and organs were harvested. Organ biodistribution was assessed for each substrate in the NTR^- and the NTR^+ groups. Fluorescence intensities were measured and analysed as explained above. The reported values were normalised by the sum of the radiance values for all organs and they were presented as the percentage of biodistributed substrate in the organs of interest.

2.9. Statistics

Results are given as mean ± standard deviation (SD). All statistical tests were performed using GraphPad Prism v 6.0 h (GraphPad Software Inc) and $p < 0.05$ was considered significant. After randomisation, a one-way ANOVA was applied to ensure unbiased assignment of tumour volumes among the experimental groups. Comparison of means was performed using Student's t-test and one-way ANOVA.

3. Results and discussion

3.1. Synthesis of 1–4

Detailed discussion of the different synthetic approaches for **1**–**4**, purification strategies and characterisation by ^{1}H NMR and high-resolution mass spectrometry (HRMS) are provided in the electronic supplementary material (Figures S1 to S22).

3.2. Spectroscopic properties and performance of the four NTR substrates in an enzymatic assay

After 2 h incubation with NTR, absorbance, excitation and emission spectra (Figure S24C and Fig. 3A) revealed overlapping excitation and emission maxima for **1** and **2** and higher, red-shifted properties for **3** and **4**, which presented the highest bathochromic shift and the largest Stokes shift (Table 1). For **3**, this far-red shift is a result of the introduction of the methoxy groups, while for **4**, this can be attributed to both the sulfonate group and the lower planarity of cyanines compared to the squaraine derivatives, which renders substrate **4** less conformationally restricted [17]. It was also observed that **1** and **2** exhibit an emission intensity in the same range as their corresponding excitation, although **2** exhibits a markedly lower absolute fluorescence intensity. **3** and **4**, however, exhibit high excitation intensities but very low emission intensities (Table 1). The UV–vis–NIR absorbance spectra of the quenched substrates and the vis-NIR absorbance spectra of the reduced substrates can be found in the electronic supplementary material (Figure S24).

From the excitation and emission spectra, the optimal fluorescence settings for each substrate were selected to perform a kinetic assay in which the fluorescence intensity was monitored for 24 h. As shown in Fig. 3B, **1**, **3** and **4** displayed a similar kinetic profile reaching the maximum fluorescence emission intensity at around 0.75 h, while maximum fluorescence for **2** was reached after 7 h. Of note, **1** exhibits the steepest reduction in fluorescence intensity of all the examined substrates (Fig. 3C). Interestingly, despite the low absolute fluorescence intensity of **2**, this is the substrate with the highest ratio of emission intensity at any given time between the reference and the sample, mainly due to the low fluorescence background it exhibits in the presence of NADH and NADPH (Fig. 3C). The three other substrates showed higher non-specific activation by the NADH and NADPH present in the mixture. All the data suggest that the four fluorescent probes are suitable substrates of NTR and worthy of biological evaluation in cell cultures.

3.3. in vitro performance of the four NTR substrates

The suitability of the four substrates for intracellular interrogation of NTR expression was assessed by incubation of NTR^{-} and NTR^{+} MDA-MB-231 cells with different substrate concentrations (1–25 μM), followed by flow cytometry analysis (Fig. 4A). The mean fluorescence intensity (MFI) of the NTR^{+} cells increased with increasing concentrations of the substrates, plateauing at 12 μM for **1** and **2**. In contrast, a plateau was not observed for **3**, demonstrating a high dependence of this substrate on the concentration. Indeed, MFI values of around 12×10^{3} were obtained with 1 μM of **2** and 3 μM of **1**, while 12 μM of **3** were required to obtain MFI in the same range. The MFI of NTR^{-} cells was notably lower but also increased with increasing concentrations of the substrates, except for **2** where a maximum was reached at 12 μM. 4 performed poorly at any given concentrations in both cell types. For **2**, NTR^{+}/NTR^{-} ratios were very similar at all concentrations whereas for **1** and **3** the highest ratios were achieved at 12 μM, due to a higher MFI of the NTR^{+} cells for **1** and a reduced MFI of the NTR^{-} cells for **3**, at this concentration. Substrate **3** shows the highest NTR^{+}/NTR^{-} ratios followed by **1** and **2** with comparable ratios.

In order to examine the dependency of MFI on incubation times, the suboptimal concentration of 3 μM was chosen and different incubation times (0.25 h–8 h) were assessed (Fig. 4B). For the NTR^{-} cells, the MFI showed a similar trend for the four different substrates with the highest values observed at the longest incubation times. Non-specific activation of the substrates was observed, however not significantly higher compared to the unstained cells (Figure S25). For the NTR^{+} cells, the fluorescence intensity of **1** and **3** plateaued at 2 h, in accordance with the observations in the kinetic enzymatic assay where the fluorescence intensity started to decrease after 3 h. The results for **2** are also in accordance with the delayed reduction reaction observed during the kinetic assay (Fig. 3B), with MFI values reaching the maximum at 8 h, although in the same range for two, four and 8 h. Interestingly, the NTR^{+}/NTR^{-} ratios for all substrates did not increase with increasing incubation times, reaching their maximum after 0.5 h.

Based on the spectroscopic data, similar fluorescence behaviour was expected for **3** and **4**, however, as can be seen in Fig. 4A and B, the sulfonated **4** exhibited almost no fluorescence enhancement at any of the given conditions. In contrast, substrate **3** resulted in modest MFI values when incubated in NTR^{-} cells and a high fluorescence enhancement in NTR^{+} cells, rendering this substrate around 200 times brighter after reduction (Fig. 4B). **1** and **2** showed comparable results, both under concentration- and time-dependent conditions, with NTR^{+}/NTR^{-} ratios in the same range.

The flow cytometry results suggest different substrate-cell interactions and confocal fluorescence microscopy was performed to investigate the intracellular behaviour of the substrates. Qualitative analysis of the fluorescence live imaging of NTR^{+} cells incubated with the different substrates (3 μM) corroborated the previous observations, yielding **1** and **2** as the brightest substrates and highlighting the low emission intensity from **3** and **4** (Figure S23). As can be seen in Fig. 5, substrate **4** required longer incubation times for the signal to be observed. From the images obtained, cellular accumulation of this substrate occurred in discrete vesicle-like structures, in contrast to the more homogeneous staining observed for the other substrates. **1**, **2** and **3** displayed homogeneous perinuclear staining. While the localisation of these three substrates was the same, the kinetics of accumulation of **3** differed from the others. The first two substrates appear to sustain comparable fluorescence intensity during 4 h of incubation, while the fluorescence intensity of **3** starts decaying after 90 min of incubation, in line with the steeper decrease in MFI observed in flow cytometry (see Videos S1–S4 for full time lapse for each substrate). To get a clearer idea of the biological behaviour of these substrates, in particular regarding tumour biodistribution, they were further investigated in murine xenograft models.

3.4. in vivo biodistribution

To understand the pharmacokinetic properties of these substrates, *in vivo* biodistribution studies over a course of 24 h were performed and compared in a subcutaneous xenograft model. Mice bearing NTR^{-} or NTR^{+} subcutaneous tumours in the scapular region (indicated by the pink sphere in Fig. 6A) were intravenously injected with 100 μL of a 1 mM substrate solution and imaging was performed at the optimal excitation and emission wavelengths for each substrate ($n = 3$ per substrate and cell type). As shown in Fig. 6A, fluorescence from the NTR^{+} tumours was observed 0.75 h post-intravenous administration with the exception of **2**, whose signal became obvious 2 h post-injection.

Radiance decreased with time for substrates **1**, **3** and **4** after 0.75 h, 2 h and 0.75 h respectively, and increased with time for substrate **2** reaching the maximum at 8 h (Fig. 6B). As seen in Fig. 6C, the best contrast (dashed black box in Fig. 6C) for **1** and **3** was observed 0.75 h post-injection, with NTR^{+}/NTR^{-} ratios of 1.5 and 1.8 respectively, and after 2 h for **2** with an NTR^{+}/NTR^{-} ratio of 1.3. These time points were employed for longitudinal imaging. The fluorescence intensity of **4** was consistently higher in NTR^{-} compared to NTR^{+} tumours at all time points studied (Fig. 6B), thus it was excluded from further *in vivo* experiments. Interestingly, strong fluorescence intensity decay was observed for **1** after 0.75 h, in accordance with the observations *in vitro*.

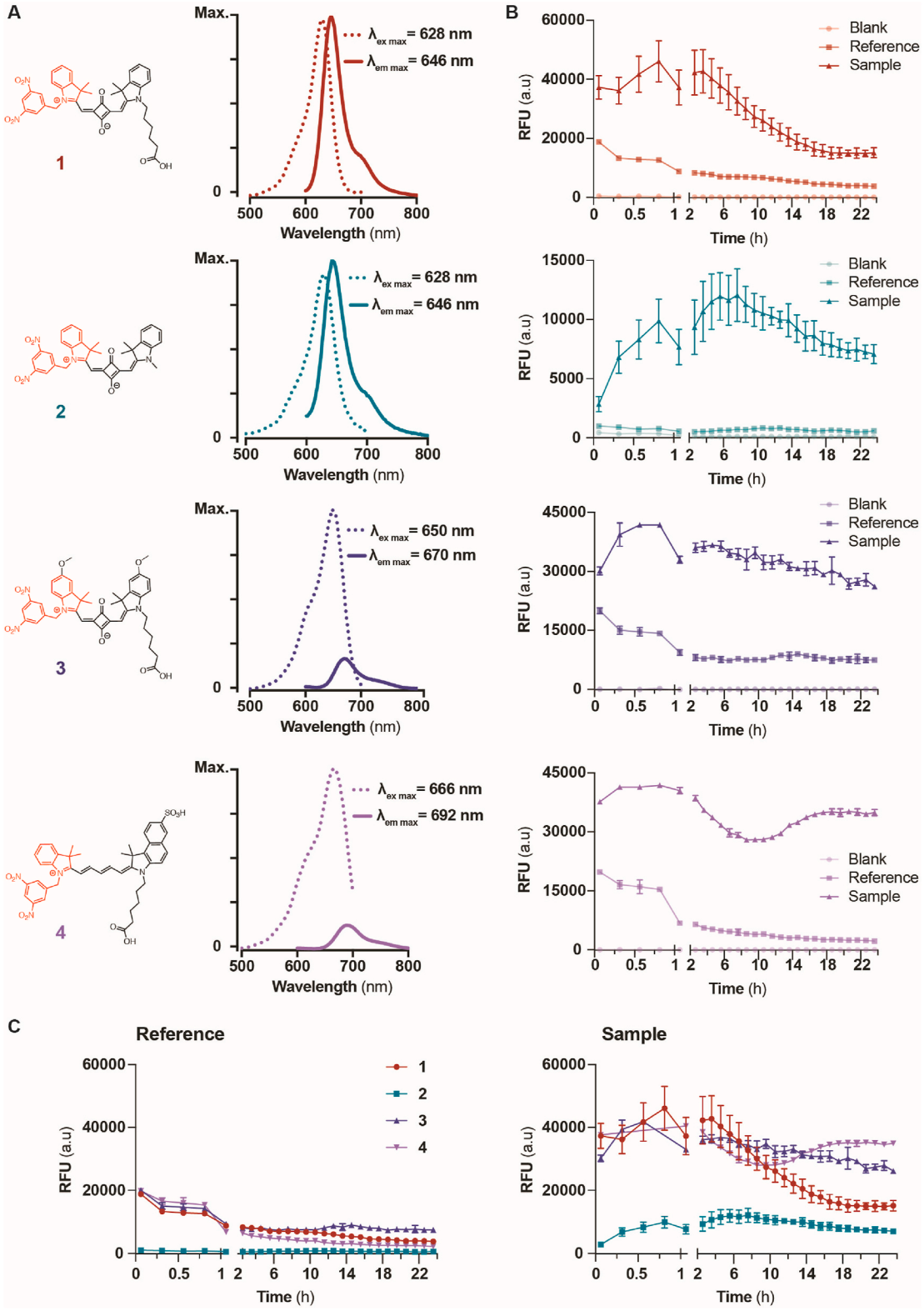

Fig. 3. Spectral characterisation of substrates **1**–**4**

A) Chemical structures of substrates **1**–**4** and their respective excitation and emission spectra after 2 h incubation of 4 μM of substrate and 0.2 μM NTR enzyme. The Y axis represents both the excitation and emission fluorescence intensity maxima expressed in Relative Fluorescence Units (RFU) for each substrate. For each dye the maximum of the scale is adjusted to the highest excitation RFU as follows: **1** (Max: 19000 RFU), **2** (Max: 4500 RFU), **3** (Max: 25000 RFU) and **4** (Max: 210000 RFU). **B)** Kinetic assessment of NTR reduction of the four different substrates, starting 3 min after NTR addition and over 24 h, expressed in Relative Fluorescence Units (RFU) as arbitrary units (a.u.). Blank consists of DMSO, β-NADH and β-NADPH in Tris-HCl buffer and NTR (0.2 μM). Reference contains DMSO, β-NADH and β-NADPH in Tris-HCl buffer and substrate under study (4 μM). Sample is composed of DMSO, β-NADH and β-NADPH in Tris-HCl buffer, substrate under study (4 μM) and NTR (0.2 μM). **C)** Overlay of the four different reduction kinetic curves for the reference and the sample, for easier visual comparison of the fluorescence intensity of the different substrates before and after reduction. From 3 min after enzyme addition and up to 24 h.

Table 1
General spectroscopic properties from the substrates under study.

Substrate	Excitation max. (nm)	Emission max. (nm)	Stokes Shift (nm)	Excitation intensity (RFU)	Emission intensity (RFU)
1	628	646	18	18500	18800
2	628	646	18	3000	4300
3	650	670	20	25000	4300
4	666	692	26	205000	28000

Also, the decrease in fluorescence emission of **3** after 2 h is in line with the fluorescence decay observed by confocal microscopy (Fig. 5).

3.5. Longitudinal tumour imaging

Further longitudinal FLI studies were performed at different mean tumour volumes, with the selected incubation times for each substrate. Mice bearing NTR^- and NTR^+ tumours (n = 6 per substrate and cell type) were injected with the three different substrates under study (**1**–**3**) and imaged 0.75 h or 2 h after injection (Fig. 7A).

For **1** and **2** average radiance was significantly higher in the NTR^+ group at any mean tumour volumes. NTR^+/NTR^- ratios through the longitudinal image range for **1** from 1.7 ± 0.5 to 2.1 ± 0.2 (p-values from 0.01 to 0.0001) and for **2** from 1.3 ± 0.2 to 2.2 ± 0.4 (p-values from 0.05 to 0.0001). In the case of **3**, no significant differences in average radiance were observed until mean tumour volumes reached 450 mm^3 when NTR^+/NTR^- ratio was 1.9 ± 0.6 ($p < 0.01$) (Fig. 7B). As observed in Fig. 4A, substrate **3** requires higher concentrations (12 μM) to achieve fluorescence intensities in the range of those obtained with 3 μM of **1** or 1 μM of **2**. It was also observed that, due to the low brightness of substrate **3**, fluorescence intensities after 0.75 h were closer to background fluorescence than those from the other two substrates. NTR^+/background ratios for substrates **1**, **2** and **3** were 3.8 ± 2.1, 14.0 ± 5.9 and 2.9 ± 1.3, respectively. From these results it can be concluded that tumour contrast increased with the increase of the mean tumour volumes for all substrates. The quantitative comparison of fluorescence intensity as a function of time in NTR^+ vs. NTR^- xenografts over the progression of the tumours allowed us to conclude that **1** is the best substrate for *in vivo* NTR interrogation even at small tumour volumes, with the highest significance between groups.

3.6. ex vivo biodistribution

To acquire a deeper understanding of the substrates' biodistribution, 0.75 h post-injection of 100 μL of a 1 mM solution of **1** and **3** and 2 h post-injection of **2**, NTR^- and NTR^+ tumour-bearing mice were euthanised, their organs excised and imaged (Fig. 7C). The percentage of biodistributed substrate was calculated and plotted in Fig. 7D. Consistent with the *in vivo* observations (Fig. 6A) high hepatobiliary uptake is observed for **1** and particularly for **3**, compatible with their highly lipophilic character. **1** also exhibits high fluorescence signal in the gastrointestinal tract with uptake in the stomach and with high uptake in the large intestine, due to activation by bacterial nitroreductases present in the GI tract [8,33]. **2** exhibits a homogeneous accumulation pattern in all organs, without clear hepatobiliary or renal excretion pathway evidence, and with a slightly higher accumulation in NTR^+ tumours compared to other organs. Residual signal is also observed for substrate **2** in control organs such as muscle and in mitochondria-enriched tissues, with known nitroreductase activity [44], such as the interscapular brown adipose tissue.

4. Conclusions

We have previously demonstrated that CytoCy5S is useful for non-invasive preclinical NIR NTR reporter gene imaging in cancers *in vivo* [8]. In the present study, we set out to clarify an ongoing discrepancy

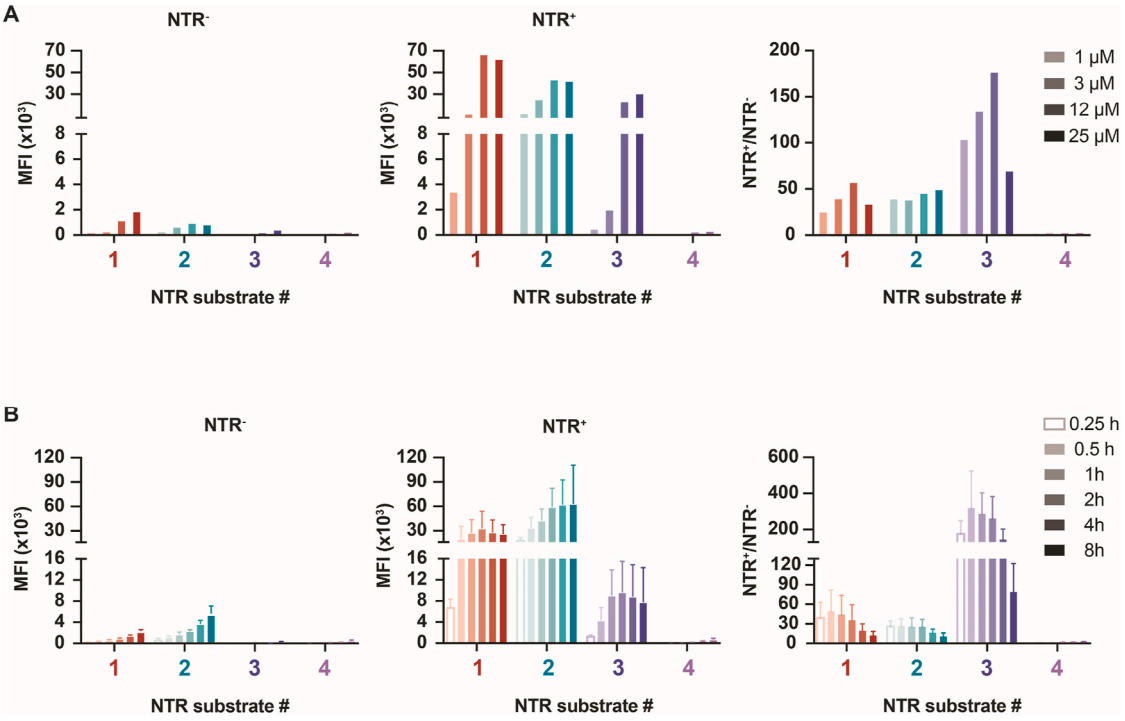

Fig. 4. Flow cytometry analysis
A) Dose-dependent fluorescence intensity was assessed by incubation of NTR^- and NTR^+ cells for 1 h with increasing concentrations of the four substrates. Values are reported as Mean Fluorescence Intensity (MFI). NTR^+/NTR^- ratios represented for each substrate at the different studied concentrations. **B)** With 3 μM, time-dependent fluorescence intensity was determined at different incubation times with NTR^- and NTR^+ cells (0.25 h, 0.5 h, 1 h, 2 h, 4 h and 8 h). NTR^+/NTR^- ratios represented for each substrate at the different studied time points.

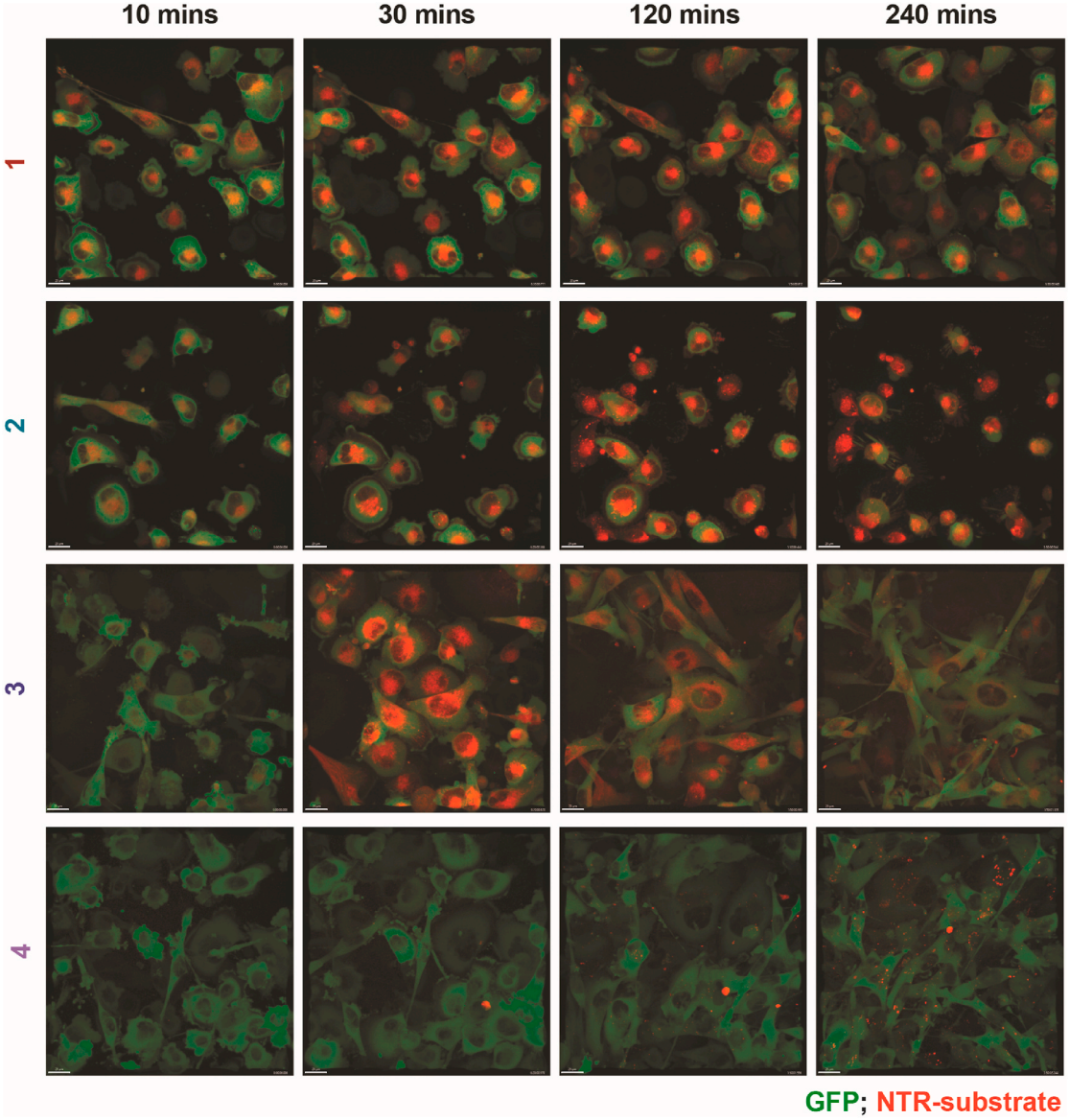

Fig. 5. Live cell fluorescence confocal microscopy imaging.
Uptake, fluorescence enhancement and localisation of the NTR-reduced metabolites were assessed over time and up to 4 h.
Cells were incubated with 3 μM of each substrate for 10 min and sequential images were acquired every 10 min for 240 min. Images of the most representative time points are presented as the merged images of the green channel (GFP; excitation: 488 nm and emission: 500–550 nm) and far-red channel (NTR-substrate; excitation: 637 nm and emission: 663–738 nm) obtained at 40X magnification. GFP is included to allow localisation of the cells in the field of view. Images are displayed in the optimal far-red channel intensity for each of the substrates. A video with the complete time-lapse for each substrate is included in the electronic supplementary material (Video S1 – S4).

regarding the structure and physicochemical properties of CytoCy5S in order to establish which of the structures denoted CytoCy5S is best suited for preclinical studies in oncology models.

The introduction of the methoxy group in **3** and the sulfonate and cyanine scaffold in **4** resulted in a modest bathochromic shift compared to **1** and **2**. All compounds were confirmed as NTR substrates with delayed kinetics observed for **2** and low emission intensities for **3** and **4**. *in vitro,* **3** was found to display the highest NTR^{+}/NTR^{-} ratio, followed by **1**.**4** performed poorly *in vitro* and *in vivo*. These results are in line with previous studies which reported that due to the contribution of the sulfonate group to increased fluorescent probe polarity these compounds exhibit limited lipid bilayer penetrance [45,46]. Despite its promising performance *in vitro*, **3** did not prove useful for discerning between NTR^{-} and NTR^{+} until tumours reached 450 mm^3 due to the limited brightness of this substrate *in vivo*. This substrate might benefit from an increase in concentration for *in vivo* applications, and although this may yield better imaging results, the cost may make *in vivo* use of this probe impracticable. **1** and **2** provided similar suitability for NTR interrogation, being **1** slightly more sensitive at smaller tumour volumes and presenting faster kinetics.

In conclusion, the spectral and biological properties of substrates **1**–**4** have been discerned and compared. NIR dye **1** was found to be best suited for imaging of NTR, both *in vitro* and *in vivo*, with superior kinetics and lower background fluorescence from surrounding tissues allowing a better delineation of tumours in our model than **2**. The latter result could potentially be explained by **2** having a methyl group and thus is expected to more easily permeate across cell membranes. Another key advantage of **1** over **2** is the presence of the carboxylic functionality, which can be exploited for further derivatisation or conjugation to biomolecules of interest for biomarker interrogation, making substrate **1** the ideal

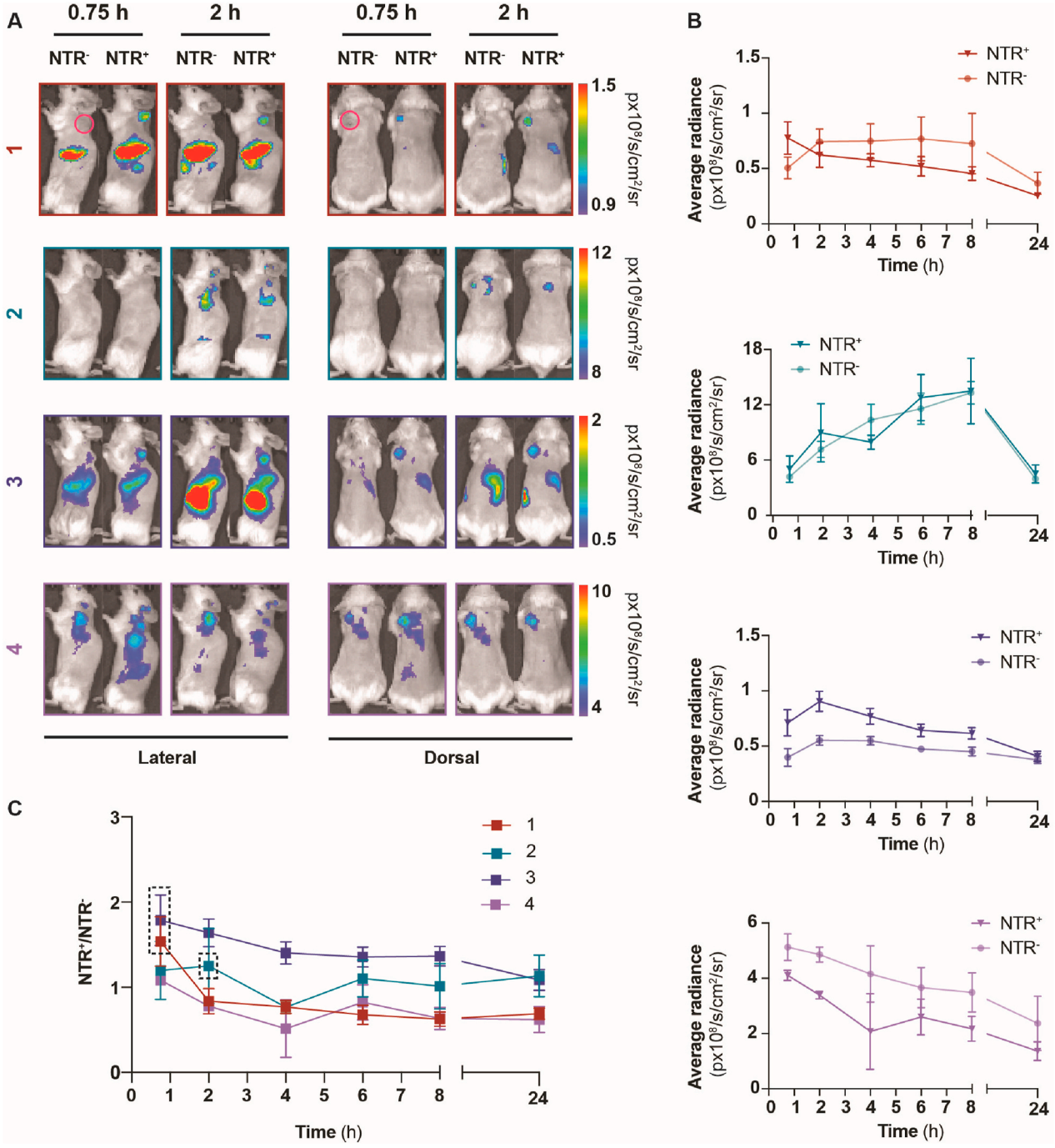

Fig. 6. *in vivo* pharmacokinetic assessment
A) NIR FLI of NTR$^-$ and NTR$^+$ xenografts (n = 3 per group per substrate) at the two most representative time points acquired, one and 2 h, after i.v. injection of 100 μL of a 1 mM substrate solution. Accumulation in the NTR$^+$ tumours is observed after 1-h injection of **1** and **3** and after 2 h for **2**. Substrate **4** accumulates indistinctly in NTR$^-$ and NTR $^+$ tumours at both time points. **B)** Fluorescence intensity of NTR$^-$ and NTR $^+$ tumours over time and up to 24 h for each substrate. Data expressed as radiance in px10^8/s/cm^2/sr. For substrate **4**, fluorescence intensity is consistently higher in NTR$^-$ than in NTR $^+$ xenografts. **C)** NTR$^+$/NTR$^-$ ratios calculated to determine the time point with the best contrast for each substrate. One hour for **1** and **3** and 2 h for **2** (dashed black box) were found optimal.

candidate for further studies. Although the substrates have been investigated in an oncology model we believe that these results can be extrapolated to other uses as already shown elsewhere [24].

Author contributions

E.G.J., B.E.H. and E.M.C. conceived and designed the study. E.G.J. performed the chemistry work supervised by B.E.H.. E.G.J. and G.R.G. performed the *in vitro* and *in vivo* work. E.G.J. wrote the manuscript and G.R.G, E.M.C. and B.E.H. contributed to writing and editing the manuscript. E.M.C. and B.E.H. were responsible for the funding acquisition. All authors have read and agreed to the published version of the manuscript.

Declaration of competing interest

The authors declare that they have no known competing financial interests or personal relationships that could have appeared to influence

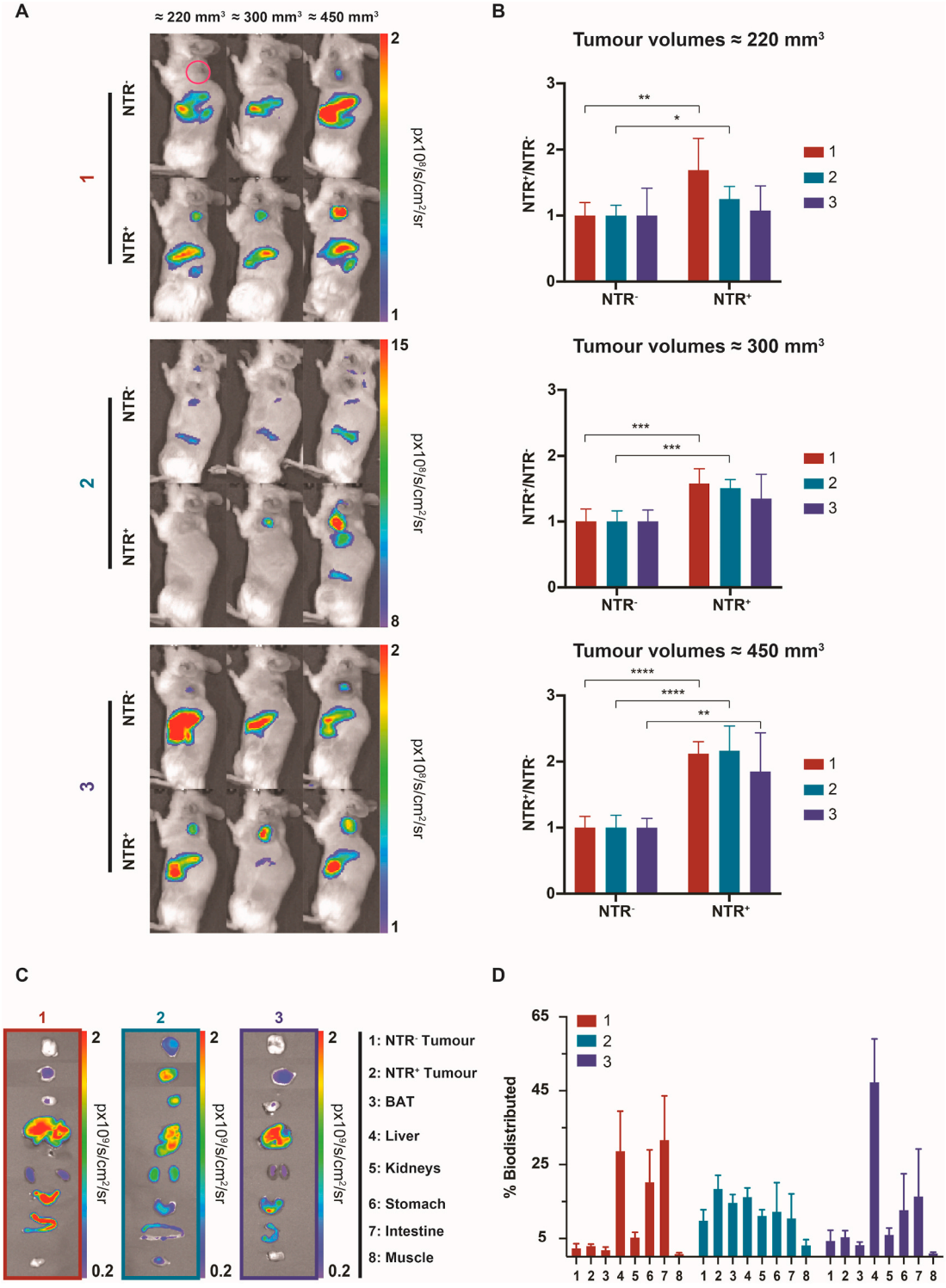

Fig. 7. Longitudinal *in vivo* optical imaging of MDA-MB-231 NTR$^-$ and NTR $^+$ subcutaneous xenografts and *ex vivo* biodistribution
A) Representative NIR fluorescence images of NTR$^-$ and NTR$^+$ xenografts (n = 6 per group and substrate) at different mean tumour volumes. **B)** NTR$^+$/NTR$^-$ ratios calculated for the different mean tumour volumes. For **1** and **2**, average radiance was significantly higher in the NTR$^+$ group at any mean tumour volume (with *p*-values: **, $p < 0.01$ and *, $p < 0.05$ respectively at 220 mm^3; ***, $p < 0.001$ for both at 300 mm^3 and ****, $p < 0.0001$ for both at 450). The NTR$^-$ and NTR $^+$ groups imaged with **3** showed no significant differences in average radiance until mean tumour volumes reached 450 mm^3 (**, $p < 0.01$). **C)** *ex vivo* biodistribution assessment after i.v. injection of 100 μL of a 1 mM substrate solution. Values expressed as radiance in px10^9/s/cm^2/sr. 1: NTR$^-$ tumour; 2: NTR$^+$ tumour 3: Interscapular brown adipose tissue (BAT); 4: Liver; 5: Kidneys; 6: Stomach; 7: Intestine; 8: Muscle. **D)** *ex vivo* biodistribution of the different substrates represented as % of sum average radiance in all organs. It shows hepatobiliary clearance of **1** and **3** and high biodistribution of the former in the gastrointestinal tract. **2** biodistributes, to all organs studied, in a more homogenous manner than the other two substrates. Higher biodistribution in NTR$^+$ tumours than in NTR$^-$ was observed in all instances.

the work reported in this paper.

Acknowledgements

The authors would like to thank Constance de Villardi de Montlaur for technical assistance with the animal work. Flow cytometry analysis was performed at the Flow Cytometry Core Facility, fluorescence microscopy was carried out at the Molecular Imaging Center (MIC) and all the *in vivo* work was performed at the animal facility in Vivarium, Department of Clinical Medicine, University of Bergen. The authors thank Brith Bergum for excellent flow cytometry technical support. Bjarte Holmelid is thanked for the technical support with the HRMS spectra acquisition and for the insightful discussions regarding optimal MS conditions. Jarl Underhaug is thanked for technical assistance with NMR. This work was partly supported by the Research Council of Norway through the Norwegian NMR Platform, NNP (226244/F50). Funding sources are acknowledged for making this work possible, University of Bergen (815900), The Norwegian Cancer Society (182735), The Research Council of Norway through its Centres of Excellence funding scheme (223250, 262652 and SonoCURE grant no. 250317), Helse Vest RHF and Helse Bergen HF (911809, 911852, 912171, 240222, 911974, HV1269). Elvira García de Jalón was the recipient of a MedIm bridging grant from the Norwegian Research School in Medical Imaging.

Appendix A. Supplementary data

Supplementary data to this article can be found online at https://doi.org/10.1016/j.dyepig.2021.109553.

References

[1] Martelli C, Lo Dico A, Diceglie C, Lucignani G, Ottobrini L. Optical imaging probes in oncology. Oncotarget 2016;7(30):48753.
[2] Li M, Wang Y, Liu M, Lan X. Multimodality reporter gene imaging: construction strategies and application. Theranostics 2018;8(11):2954–73.
[3] Shaikh FA, Kurtys E, Kubassova O, Roettger D. Reporter gene imaging and its role in imaging-based drug development. Drug Discov Today 2020;25(3):582–92.
[4] Luo SL, Zhang EL, Su YP, Cheng TM, Shi CM. A review of NIR dyes in cancer targeting and imaging. Biomaterials 2011;32(29):7127–38.
[5] Owens EA, Lee S, Choi J, Henary M, Choi HS. NIR fluorescent small molecules for intraoperative imaging. Wiley Interdiscip Rev Nanomed Nanobiotechnol 2015;7(6):828–38.
[6] Jacques SL. Optical properties of biological tissues: a review. Phys Med Biol 2013;58(11):R37–61.
[7] Owens EA, Henary M, El Fakhri G, Choi HS. Tissue-specific near-infrared fluorescence imaging. Accounts Chem Res 2016;49(9):1731–40.
[8] McCormack E, Silden E, West RM, Pavlin T, Micklem DR, Lorens JB, et al. Nitroreductase, a near-infrared reporter platform for in vivo time-domain optical imaging of metastatic cancer. Cancer Res 2013;73(4):1276–86.
[9] van Dam GM, Themelis G, Crane LMA, Harlaar NJ, Pleijhuis RG, Kelder W, et al. Intraoperative tumor-specific fluorescence imaging in ovarian cancer by folate receptor-alpha targeting: first in-human results. Nat Med 2011;17(10):1315–9.
[10] Zhu B, Wu G, Robinson H, Wilganowski N, Hall MA, Ghosh SC, et al. Tumor margin detection using quantitative NIRF molecular imaging targeting EpCAM validated by far red gene reporter iRFP. Mol Imag Biol 2013;15(5):560–8.
[11] Hoogstins CES, Tummers QRJG, Gaarenstroom KN, de Kroon CD, Trimbos JBMZ, Bosse T, et al. A novel tumor-specific agent for intraoperative near-infrared fluorescence imaging: a translational study in healthy volunteers and patients with ovarian cancer. Clin Canc Res 2016;22(12):2929–38.
[12] Kleinmanns K, Fosse V, Davidson B, de Jalon EG, Tenstad O, Bjorge L, et al. CD24-targeted intraoperative fluorescence image-guided surgery leads to improved cytoreduction of ovarian cancer in a preclinical orthotopic surgical model. EBioMedicine 2020;56:102783.
[13] Li X, Yu S, Lee Y, Guo T, Kwon N, Lee D, et al. In vivo albumin traps photosensitizer monomers from self-assembled phthalocyanine nanovesicles: a facile and switchable theranostic approach. J Am Chem Soc 2019;141(3):1366–72.
[14] Tsolekile N, Nahle S, Zikalala N, Parani S, Sakho EHM, Joubert O, et al. Cytotoxicity, fluorescence tagging and gene-expression study of CuInS/ZnS QDS - meso (hydroxyphenyl) porphyrin conjugate against human monocytic leukemia cells. Sci Rep 2020;10(1):4936.
[15] Gawale Y, Adarsh N, Kalva SK, Joseph J, Pramanik M, Ramaiah D, et al. Carbazole-linked near-infrared aza-BODIPY dyes as triplet sensitizers and photoacoustic contrast agents for deep-tissue imaging. Chemistry 2017;23(27):6570–8.
[16] Zhu S, Tian R, Antaris AL, Chen X, Dai H. Near-infrared-II molecular dyes for cancer imaging and surgery. Adv Mater 2019;31(24):e1900321.
[17] Tong L, Bi-Xian P, Fenglian B. The structure and 13C-NMR of an indolenium squaraine dye. Dyes Pigments 1999;43(2):67–71.
[18] Zhu H, Fan J, Mu H, Zhu T, Zhang Z, Du J, et al. D-PET-controlled "off-on" polarity-sensitive probes for reporting local hydrophilicity within lysosomes. Sci Rep 2016;6(1):35627.
[19] Murata O, Shindo Y, Ikeda Y, Iwasawa N, Citterio D, Oka K, et al. Near-infrared fluorescent probes for imaging of intracellular Mg2+ and application to multi-color imaging of Mg2+, ATP, and mitochondrial membrane potential. Anal Chem 2020;92(1):966–74.
[20] Lee H, Akers W, Bhushan K, Bloch S, Sudlow G, Tang R, et al. Near-infrared pH-activatable fluorescent probes for imaging primary and metastatic breast tumors. Bioconjugate Chem 2011;22(4):777–84.
[21] Lacivita E, Leopoldo M, Berardi F, Colabufo NA, Perrone R. Activatable fluorescent probes: a new concept in optical molecular imaging. Curr Med Chem 2012;19(28):4731–41.
[22] Klockow JL, Hettie KS, LaGory EL, Moon EJ, Giaccia AJ, Graves EE, et al. An activatable NIR fluorescent rosol for selectively imaging nitroreductase activity. Sensor Actuator B Chem 2020;306:127446.
[23] Wei C, Shen Y, Xu Z, Peng S, Yuan Z, He Y, et al. A novel off-on fluorescent probe for imaging of hypoxia in tumor cell. J Photochem Photobiol, A 2018;353:292–8.
[24] Stanton M, Cronin M, Lehouritis P, Tangney M. In vivo bacterial imaging without engineering; A novel probe-based strategy facilitated by endogenous nitroreductase enzymes. Curr Gene Ther 2015;15(3):277–88.
[25] Welling MM, Hensbergen AW, Bunschoten A, Velders AH, Scheper H, Smits WK, et al. Fluorescent imaging of bacterial infections and recent advances made with multimodal radiopharmaceuticals. Clin Transl Imaging 2019;7(2):125–38.
[26] Zhang L, Guo L, Shan X, Lin X, Gu T, Zhang J, et al. An elegant nitroreductase responsive fluorescent probe for selective detection of pathogenic Listeria in vitro and in vivo. Talanta 2019;198:472–9.
[27] Huang B, Chen W, Kuang Y-Q, Liu W, Liu X-J, Tang L-J, et al. A novel off–on fluorescent probe for sensitive imaging of mitochondria-specific nitroreductase activity in living tumor cells. Org Biomol Chem 2017;15(20):4383–9.
[28] Djeha AH, Hulme A, Dexter MT, Mountain A, Young LS, Searle PF, et al. Expression of Escherichia coli B nitroreductase in established human tumor xenografts in mice results in potent antitumoral and bystander effects upon systemic administration of the prodrug CB1954. Canc Gene Ther 2000;7(5):721–31.
[29] Smits AM, van den Hengel LG, van den Brink S, Metz CH, Doevendans PA, Goumans M-J. A new in vitro model for stem cell differentiation and interaction. Stem Cell Res 2009;2(2):108–12.
[30] Thorne SH, Barak Y, Liang W, Bachmann MH, Rao J, Contag CH, et al. CNOB/ChrR6, a new prodrug enzyme cancer chemotherapy. Mol Canc Therapeut 2009;8(2):333.
[31] Parkinson GN, Skelly JV, Neidle S. Crystal structure of FMN-dependent nitroreductase from Escherichia coli B: A prodrug-activating enzyme. J Med Chem 2000;43(20):3624–31.
[32] Johansson E, Parkinson GN, Denny WA, Neidle S. Studies on the nitroreductase prodrug-activating system. Crystal structures of complexes with the inhibitor dicoumarol and dinitrobenzamide prodrugs and of the enzyme active form. J Med Chem 2003;46(19):4009–20.
[33] Bhaumik S, Sekar TV, Depuy J, Klimash J, Paulmurugan R. Noninvasive optical imaging of nitroreductase gene-directed enzyme prodrug therapy system in living animals. Gene Ther 2012;19(3):295–302.
[34] Sekar TV, Foygel K, Ilovich O, Paulmurugan R. Noninvasive theranostic imaging of HSV1-sr39TK-NTR/GCV-CB1954 dual-prodrug therapy in metastatic lung lesions of MDA-MB-231 triple negative breast cancer in mice. Theranostics 2014;4(5):460–74.
[35] Devulapally R, Lee T, Barghava-Shah A, Sekar TV, Foygel K, Bachawal SV, et al. Ultrasound-guided delivery of thymidine kinase–nitroreductase dual therapeutic genes by PEGylated-PLGA/PEI nanoparticles for enhanced triple negative breast cancer therapy. Nanomedicine 2018;13(9):1051–66.
[36] Kanada M, Kim BD, Hardy JW, Ronald JA-OX, Bachmann MA-O, Bernard MP, et al. Microvesicle-mediated delivery of minicircle DNA results in effective gene-directed enzyme prodrug cancer therapy. Mol Canc Therapeut 2019;18(12):2331–42.
[37] West RM, Ismail R. Nitro-substituted squaraine reporter dyes as reagent for measuring nitroreductase enzyme activity (Patent No. WO2005118839A1), https://worldwide.espacenet.com/patent/search/family/032671256/publication/WO2005118839A1?q=WO2005118839A1; 2005.
[38] Thomas N, Michael NP, Millar V, Davies B, Briggs MSJ. Methods for increased fluorescence of Cyanine dye reagents with nitroreductase (Patent No. WO2001057237A2), https://worldwide.espacenet.com/patent/search/family/009884728/publication/WO0157237A2?q=WO2001057237A2; 2001.
[39] Bhaumik S, Agdeppa ED, Klimash J, Depuy JC. In vivo optical imaging (Patent No. US20090004116A1), https://worldwide.espacenet.com/patent/search/family/040160790/publication/US2009004116A1?q=US20090004116A1; 2009.
[40] 25th August Cytiva. Nitroreductase gene reporter system. 2020. https://cdn.cytivalifesciences.com/dmm3bwsv3/AssetStream.aspx?mediaformatid=10061&destinationid=10016&assetid=13959.
[41] Parker CN, Ottl J, Gabriel D, Zhang J-H. Chapter 8 advances in biological screening for lead discovery. Natural Product Chemistry for Drug Discovery: The Royal Society of Chemistry 2009:243–71.
[42] Inglese J. Measuring Biological Responses with Automated Microscopy 2006;414.
[43] Elmes RB. Bioreductive fluorescent imaging agents: applications to tumour hypoxia. Chem Commun 2016;52(58):8935–56.

[44] Chevalier A, Zhang Y, Khdour OM, Kaye JB, Hecht SM. Mitochondrial nitroreductase activity enables selective imaging and therapeutic targeting. J Am Chem Soc 2016;138(37):12009–12.
[45] Loew LM, Cohen LB, Salzberg BM, Obaid AL, Bezanilla F. Charge-shift probes of membrane-potential - characterization of aminostyrylpyridinium dyes on the squid giant-axon. Biophys J 1985;47(1):71–7.
[46] Yan Q, Schmidt BF, Perkins LA, Naganbabu M, Saurabh S, Andreko SK, et al. Near-instant surface-selective fluorogenic protein quantification using sulfonated triarylmethane dyes and fluorogen activating proteins. Org Biomol Chem 2015;13(7):2078–86.